Journal of Zhejiang University-SCIENCE A (Applied Physics & Engineering) in press
www.jzus.zju.edu.cn; www.springer.com/journal/11582
E-mail: jzus_a@zju.edu.cn

Research Article

https://doi.org/10.1631/jzus.A2300339

Comparative analysis between single-train passing and double-train intersection in a tunnel

Jianming DU[1], Qian FANG[2]✉, Xuan ZHANG[1], Hualao WANG[1]

[1]*Bridge and Tunnel Research Center, Research Institute of Highway Ministry of Transport, Beijing 100088, China*
[2]*Tunnel and Underground Engineering Research Center of Ministry of Education, Beijing Jiaotong University, Beijing 100044, China*

Abstract: Aerodynamic pressure significantly impacts the scientific evaluation of tunnel service performance. The aerodynamic pressure of two trains running in a double-track tunnel is considerably more complicated than that of a single train. We used the numerical method to investigate the difference in aerodynamic pressure between a single train and two trains running in a double-track tunnel. First, the numerical method was verified by comparing the results of numerical simulation and on-site monitoring. Then, the characteristics of aerodynamic pressure were studied. Finally, the influence of various train-tunnel factors on the characteristics of aerodynamic pressure were investigated. The results show that the aerodynamic pressure variation can be divided into Stage I: irregular pressure fluctuations before the train tail leaves the tunnel exit, and Stage II: periodic pressure decline after the train tail leaves the tunnel exit. In addition, the aerodynamic pressure simultaneously jumps positively or drops negatively for a single train or two trains running in double-track tunnel scenarios. The pressure amplitude in the two-train case is higher than that for a single train. The P_{STP}/P_{STN} (maximum positive peak pressure difference / maximum negative peak pressure difference) increases as train speed rises to the power from 2.256 to 2.930 in Stage I. The P_{STP}/P_{STN} first increases and then decreases with the increase of tunnel length in Stage I. The P_{STP}/P_{STN} increases as the blockage ratio rises to the power from 2.032 to 2.798 in Stages I and II.

Key words: Railway tunnel; Aerodynamic effect; Pressure characteristic; Train speed; Tunnel length; Blockage ratio

1 Introduction

Pressure waves caused by a train travelling through a tunnel at high speed are continuously reflected and superimposed between the tunnel entrance and exit, resulting in a series of aerodynamic pressures (Howe. 2007; Rivero et al., 2018; Saito et al., 2020). Under continuous aerodynamic pressure effects, the initial defects inside tunnel structures (such as voids and cracks) tend to further initiate, expand, and even penetrate, causing lining-structure incompletion, bearing-capability reduction, and shortening of tunnel service life (Gong and Zhu. 2018; Liu et al., 2019(b); Du et al., 2021; Du et al., 2022(c)). Therefore, aerodynamic pressure research is significant for railway tunnels.

In this study, we systematically studied the characteristics of aerodynamic pressure associated with train-tunnel factors, using theoretical analysis, a numerical method, on-site monitoring, and laboratory tests. The relevant factors included the speed and formation type of trains, the length and entrance hood of the tunnel, and the blockage ratio. For the case of a single train travelling through a tunnel, the characteristics of aerodynamic pressure associated with train speed and formation, as well as tunnel length, have been previously analyzed through field monitoring (Ko et al., 2012; Liu et al., 2019(b)). The influence of train speed and nose length, and the tunnel entrance hood, on tunnel aerodynamic pressure have been studied numerically (Chen et al., 2017(b); Du et al., 2022(a)). Within this context, a series of laboratory test was used to investigate the characteristics of aerodynamic pressure associated with train speed and formation, and the tunnel portal (Yang et al., 2016; Du et al., 2020). The effects of the tunnel entrance hood and hood geometry on tunnel

✉ Qian FANG, qfang@bjtu.edu.cn
Jianming DU, https://orcid.org/0000-0002-8148-9228
Qian FANG, https://orcid.org/0000-0002-1850-8991

Received July 1, 2023; Revision accepted Oct. 15, 2023; Crosschecked

© Zhejiang University Press 2023

unedited

aerodynamic pressure have also been explored using theoretical analysis (Howe. 2007; Howe et al., 2008; Saito. 2019). For the case of two trains intersecting in a double-track tunnel, the influence of train speed and tunnel length were examined by numerical simulation (Chu et al. 2014) and field testing (Liu et al. 2019(a)). Subsequently, the difference in the unsteady slipstream between a single train and two trains was investigated numerically (Li et al., 2020). However, characteristic comparative analysis of aerodynamic pressure between a single train and two trains has not been carried out.

Therefore, we used the numerical method to explore the difference in the characteristics of aerodynamic pressure between a single train and two trains running in a double-track tunnel. First, we verified the accuracy of the numerical method by comparing the results from numerical simulation and on-site monitoring. Then, we explored the time-history curves of aerodynamic pressure. Finally, we looked at the difference in the characteristics of aerodynamic pressure associated with train-tunnel factors for a single train and two trains running in a double-track tunnel.

2 Methodology

2.1 Models

The prototype of the train model was a CRH380 train with eight units, and the tunnel model was a double-track tunnel with an area of 100 m2. These prototypes are commonly used in high-speed railway lines in China (Chu et al., 2014; Deng et al., 2020). For the train model (as shown in Fig. 1) the height and width were respectively 3.7 and 3.38 m, the length of the head and middle cars were respectively 26.5 and 25.0 m, and the total length of the car was 203.0 m. The streamlined length of the train nose was 12.0 m. In the tunnel model, the center distance of the double track was 5.0 m. The cross-sectional area of the train model was 11.22 m^2, and of the tunnel model was 100 m^2, and the corresponding blockage ratio (γ) was 0.1122. The train model was simplified as a smooth body to improve the numerical simulation's computational efficiency while ensuring computational accuracy (Chu et al., 2014; Li et al., 2019(a)).

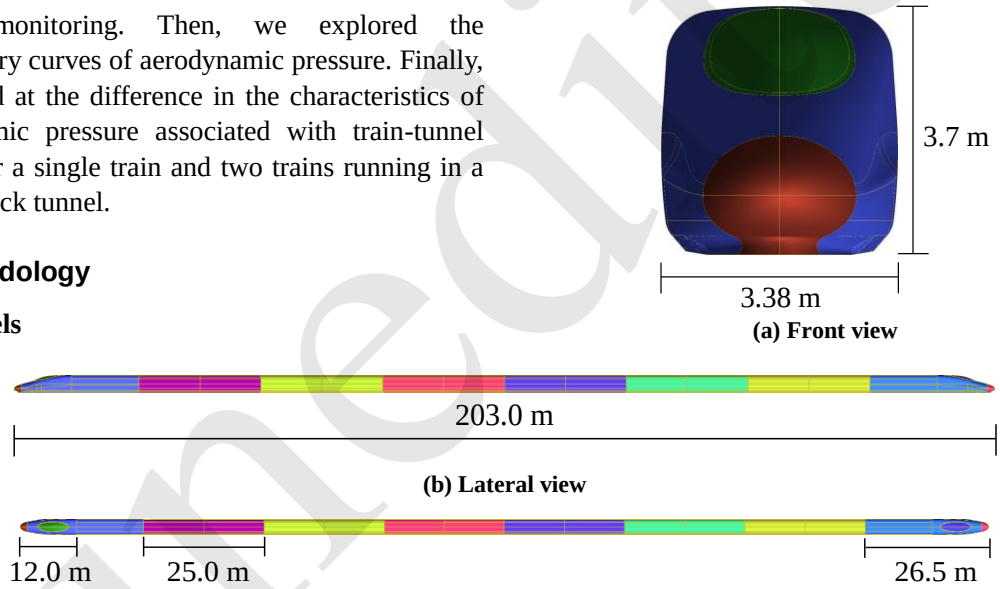

(c) Vertical view

Fig. 1 Train model (unit: m)

2.2 Model Options

The overall layout and boundary conditions of the numerical model are shown in Figs. 2 and 3, respectively. The size of the simulation domain near the tunnel entrance was similar to that near the exit. The length, width, and height were respectively, 600, 120, and 60 m, ensuring full development of the flow field in the domain (Chu et al., 2014; Lu et al., 2021; Du et al., 2022(a)). The overall numerical model was segmented into static zone 1 and dynamic zone 2. We used an interface boundary condition to implement the information exchange between zone 1 and zone 2. Sliding mesh technology was used to simulate the relative motion of the train in the tunnel (Li and Guan. 2012; Wang et al., 2018; Liu et al., 2020).

unedited

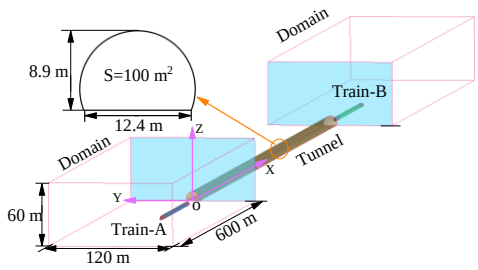

Fig. 2. Computational domain

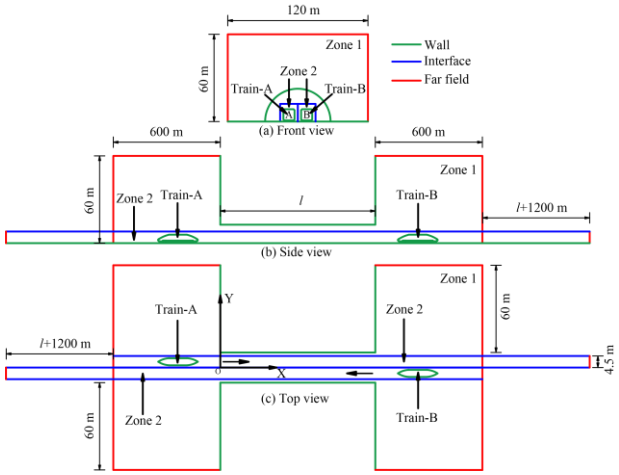

Fig. 3. Boundary conditions

The interface allowed the exchange of information between sliding zone 2 and stationary zone 1. A sketch of the information exchange on the interface is shown in Fig. 4. When the sliding grid zone 2 slid to the left, the relative motion between zone 1 and zone 2 formed a common interface. The pressure information was transmitted between zone 2-Ⅰ, 2-Ⅱ, and 2-Ⅲ and zone 1-I, 1-II, and 1-III. The number of intersectional grids on the common interface changed when interface 2 of zone 2 slid relative to interface 1 of zone 1. The pressure information travelling through the common interface was calculated by the intersectional grids on the common interface. Thus, the information could be exchanged between adjacent zones.

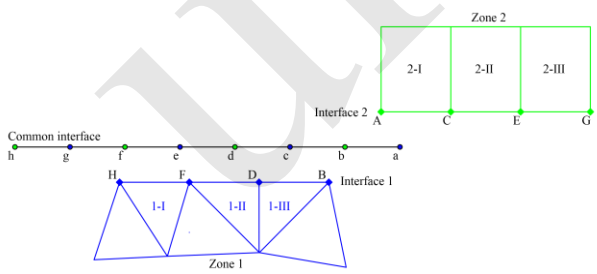

Fig. 4. Diagram of information exchange on the interface

Fig. 5 shows the time-history curves of aerodynamic pressure for different distances between the initial position of the train nose and the tunnel entrance. When the distance increased from 50.0 to 200.0 m, the difference in maximum positive and negative peak values was respectively 2.5% and 2.1%. Therefore, combining this information with the knowledge in the existing literature (Li and Guan. 2012; Lu et al., 2021), we set the distance as 50.0 m.

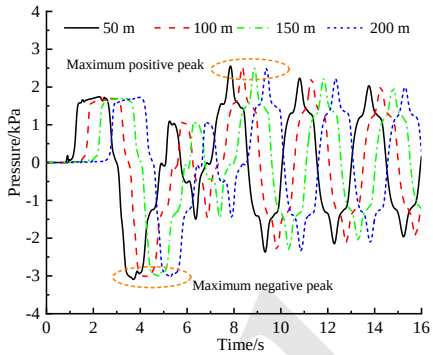

Fig. 5. Time-history curves of aerodynamic pressure for different distances between the initial position of the train nose and the tunnel entrance

2.3 Model mesh

Fig. 6 shows the mesh scheme adopted in the numerical model. The local meshes of the train nose and tunnel wall were refined to ensure computational accuracy. Mesh generation for the overall model was carried out using structured mesh technology (Liu et al., 2019(a); Liu et al., 2020; Du et al., 2022(b)) to improve the meshing quality. The quality of the near-wall mesh could be evaluated by a non-dimensionless distance y^+. The y^+ values of the train surface and the tunnel wall in our simulation were controlled between 30 and 180, which met the requirements of standard wall function (National Railway Administration of the People's Republic of China Standard. 2018). The minimum mesh sizes of the train model and tunnel model were respectively 0.0075 and 0.01 m, and the total number of meshes was 42.18 million.

We evaluated the influence of mesh density on the calculated results of numerical simulation. Three types of mesh, including fine (21.1 million cells), medium (15.5 million cells), and coarse (10.3 million cells), were selected. The train speed was set as 350 km/h, and the tunnel length was 1000 m. The time-history curves of aerodynamic pressure for the three levels of mesh density are shown in Fig. 7. The maximum peak-to-peak values of fine, medium, and coarse meshes were 3.362, 3.361, and 3.368 kPa, respectively. The difference between fine and medium mesh was smaller than that between fine and coarse mesh. Therefore, we used the medium mesh parameters in the subsequent numerical analysis.

unedited

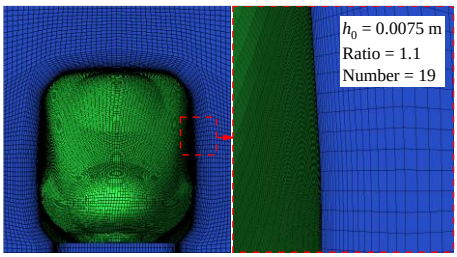

(a) train nose

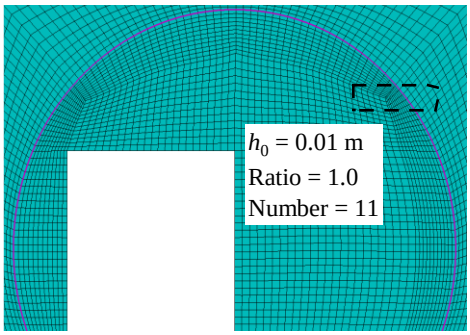

(b) tunnel portal

Fig. 6. Meshing scheme used in model

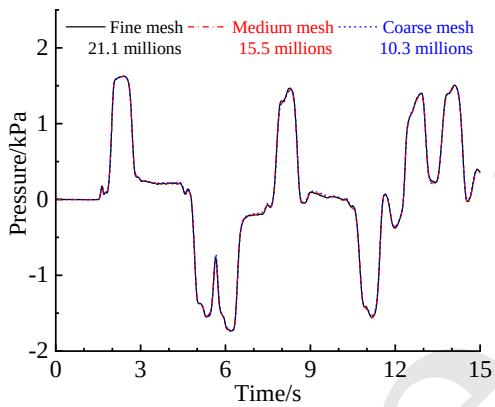

Fig. 7. Time-history curves of aerodynamic pressure for different mesh densities

2.4 Solver parameters

The RNG k-e two-equation turbulence model was used to simulate the turbulence characteristics of the flow field (Howe et al., 2008; Li et al., 2021). A finite volume-based fluid calculation software program was used to calculate the pressure and velocity. The coupling between the pressure field and velocity field was dealt with using the SIMPLE algorithm, and the pressure field update was handled using the iterative method. Meanwhile, the second-order implicit scheme was used for the non-stationary term. The time step for all numerical calculations was set as 0.001 seconds, and the maximum iteration was taken as 50.

2.5 Computed conditions

The primary train-tunnel factors in this study were the train speed (v), tunnel length (l), and blockage ratio (γ). The computed conditions of the numerical simulation are shown in Table 1. The height between the monitoring point and the ground was set as 1.5 m, while the distance between the monitoring point and the tunnel entrance was represented by its X-axis value.

Table 1 Computed conditions of the numerical simulation

ID	v (km/h)	l/m	γ
1	275	1000	0.110
2	300	1000	0.110
3	325	1000	0.110
4	350	1000	0.110
5	350	800	0.110
6	350	600	0.110
7	350	400	0.110
8	350	200	0.110
9	350	1000	0.121
10	350	1000	0.132
11	350	1000	0.143
12	350	1000	0.154
13	375	1000	0.110
14	400	1000	0.110

3 Validation

To estimate the calculation parameters and simulation results of the numerical method, we compared the calculation results with the monitoring results obtained in the field. Monitoring in the field was performed on the high-speed railway line from Beijing to Shanghai (Chen et al., 2017(b)). For actual double-track tunnel, the length and the cross-sectional area were 978.0 m and 100 m2, respectively. The monitoring points for aerodynamic pressure acting on the tunnel wall were located at a height of 1.5 m from the ground. The train type was CRH380 (with eight units), and the train speed was 300 km/h. For the numerical method, the small features of the train (such as lights, handlebars, bogies, and roof pantographs) and tunnel models were not considered, because the influence of these features on aerodynamic pressure are negligible (Du et al., 2022(a)). The other geometric dimensions of the train and tunnel models were the same as those in the field.

The comparison of aerodynamic pressure results is shown in Fig. 8. There is agreement between the time-history curves of aerodynamic pressure obtained by the two methods. The differences in the maximum positive and negative peak values for these two methods were 3.27% and 1.42% at a measuring point located 500 m away from the tunnel entrance, respectively, and 1.44% and 1.57% at a measuring point located 860 m away. Therefore, the simulation results and calculation parameters of the numerical method can be considered reasonable and reliable, and the calculation parameters can be employed in the subsequent analysis.

Unedited

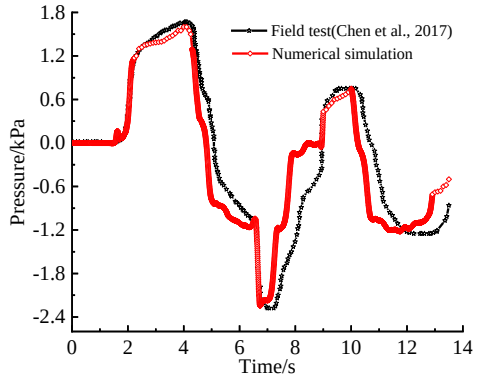

(a) Monitoring point located 500 m away from tunnel entrance

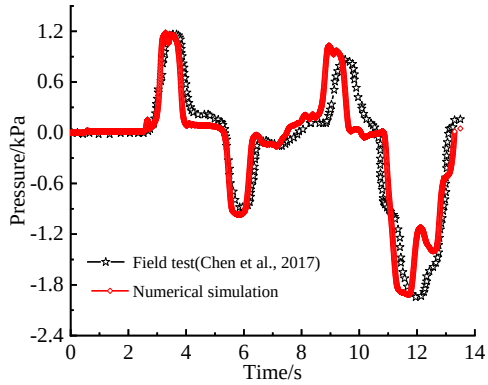

(b) Monitoring point located 860 m away from tunnel entrance

Fig. 8. Comparison of aerodynamic pressure between numerical and monitoring results

4 Results

4.1 Time-history curves of aerodynamic pressure

Fig. 9 shows the time-history curves of aerodynamic pressure in a tunnel's longitudinal middle section under different computed conditions. The aerodynamic pressure variation can be divided into Stage I and Stage II according to the change trend of the time-history curve, where Stage I corresponds to irregular pressure fluctuations before the train tail leaves the tunnel exit, and Stage II corresponds to periodic pressure decline after the train tail leaves the tunnel exit. The aerodynamic pressure simultaneously jumps positively or drops negatively in single-train and two-train cases. The pressure amplitude of positive and negative peak pressures for the two-train case is larger than that for a single train.

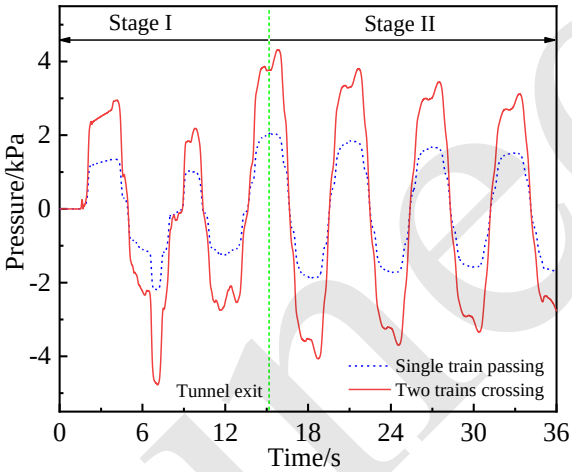

(a) computed condition 2

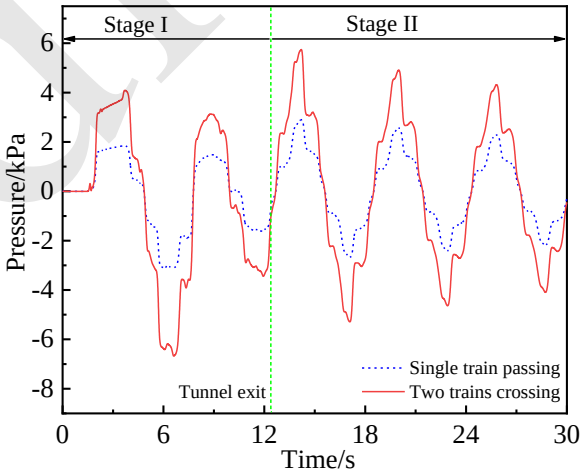

(b) computed condition 4

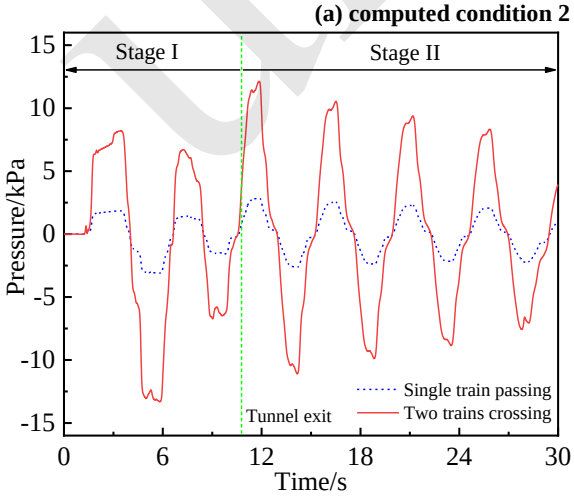

(c) computed condition 5

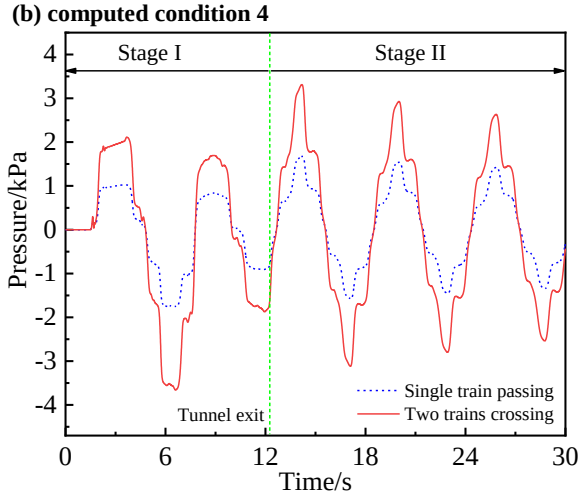

(d) computed condition 11

Fig. 9. Time-history curves of aerodynamic pressure in a tunnel's longitudinal middle section under different computed

Unedited

conditions

Fig. 10 shows the relationship between the wave diagram in the tunnel and aerodynamic pressure variation in the tunnel's longitudinal middle section for computed condition 4 (v=350 km/h l=1000 m γ=0.110). The positive jump in aerodynamic pressure is induced by a compression wave and the train tail. For example, the moment of t_1, t_4, t_5, t_7, and t_9. Similarly, the negative drop in aerodynamic pressure is induced by a rarefaction wave and the train nose. For example, the moment of t_2, t_3, t_6, and t_8.

When two train noses enter the tunnel entrance, dual pressure waves are generated and both propagate forward toward the tunnel exit. Once dual pressure waves arrive at the tunnel exit, the corresponding reflected waves are generated and both propagate forward toward the tunnel entrance. The generation and reflection process of the pressure waves caused by two trains leaving the tunnel exit are similar to that of two trains entering the tunnel entrance. Although the wave diagram for the two-train case is more complicated than that for the single-train case at the same speed, one interesting finding here is that the moments of pressure waves, and those of the train nose and tail arriving at the measuring section, such as the moment of t1 to t_9, are coincident. The corresponding result is that the aerodynamic pressures jump or drop at the same time. The single pressure wave arrives at the measuring section when a single train is running in the tunnel, while two identical pressure waves arrive simultaneously while the two trains are running in the double-track tunnel. Accordingly, the amplitude of positive and negative peak pressures for the two-train case is higher than for the single-train case.

Table 2 shows the maximum peak pressures in the tunnel's longitudinal middle section for computed condition 4 (v=350 km/h l=1000 m γ=0.110). Compared to the single-train case, the peak pressures are significantly influenced by the superimposed effect of the two-train case. For example, the maximum positive peak (MPP) pressures in the single-train and two-train cases for Stage I are 1.84 and 4.09 kPa, respectively. The maximum positive peak pressure difference (P_{STP}) between the single-train and two-train cases is 2.25 kPa, which is about 1.22 times the MPP pressure for the single-train case. The P_{STP} in Stage II between the two cases is 2.83 kPa, about 0.97 times the MPP pressure for the single-train case. Similarly, the maximum negative peak pressure difference (P_{STN}) between the two cases in Stages I and II is 3.57 and 2.83 kPa, respectively. These are 1.15 and 0.97 times the maximum negative peak (MNP) pressure for the single-train case, respectively. Hence, the superimposed effect of two trains has a larger influence on peak pressures in Stage I than in Stage II.

unedited

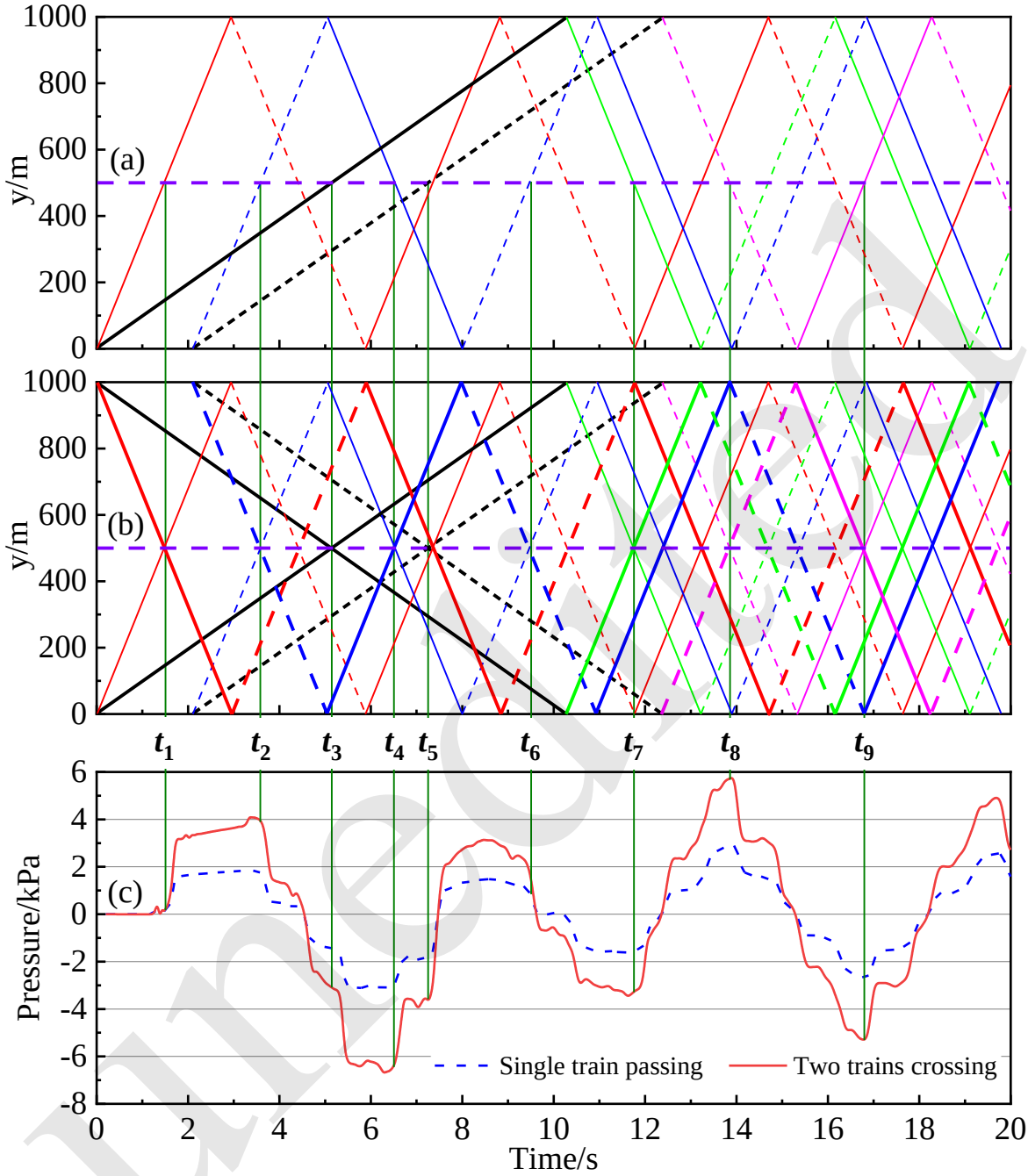

Fig. 10. Relationship between the wave diagram in the tunnel and pressure variation for computed condition 4. (a) wave diagram for single-train case (b) wave diagram for two-train case (c) Pressure variation (x=500 m) for single-train and two-train cases. The y label indicates the distance from the tunnel entrance. The solid black lines indicate the travelling path of the train nose. Dotted black lines indicate the travelling path of the train tail. Red lines represent pressure waves induced by the train nose at the tunnel entrance. Green lines represent pressure waves caused by the train nose at the tunnel exit. Except for black lines, the solid lines denote compression waves, and the dotted lines denote rarefaction waves. The thin and thick lines represent the travelling path and corresponding wave diagram of train A and train B, respectively. In addition, the vertical olive-green lines indicate the moments when the pressure waves, train nose, and train tail reached the measuring section.

Table 2 Maximum peak pressures in the tunnel's longitudinal middle section for computed condition 4 (unit: kPa)

Scenario	Stage I	Stage II

unedited

Maximum positive peak pressure	Single-train case	1.84	2.91
	Two-train case	4.09	5.74
Pressure difference (P_{STP})		2.25	2.83
Maximum negative peak pressure	Single-train case	-3.11	-2.67
	Two-train case	-6.68	-5.26
Pressure difference (P_{STN})		3.57	2.59

4.2 Train speed effect

(1) Aerodynamic pressure in Stage I

Fig. 11 shows the MPP/MNP pressure distributions along the tunnel longitudinal axis at 275 and 375 km/h train speed in Stage I (l=1000 m γ=0.110). The MPP/MNP pressure of the monitoring points near the middle section of the tunnel are generally larger than those near the tunnel portals. The P_{STP}/P_{STN} near tunnel portals are negligible. The P_{STP}/P_{STN} gradually increase from a tunnel portal to the middle section, reaching the maximum value at the tunnel's middle section. The histogram of maximum peak pressures (positive and negative) in the tunnel's longitudinal middle section at different train speeds in Stage I are shown in Fig. 12. The amplitude of the maximum peak pressure increases as train speed rises to the power from 2.202 to 2.328. The relationship between the P_{STP}/P_{STN} and train speed in Stage I is shown in Fig. 13. Similarly, the P_{STP}/P_{STN} increases as train speed rises to the power from 2.256 to 2.930.

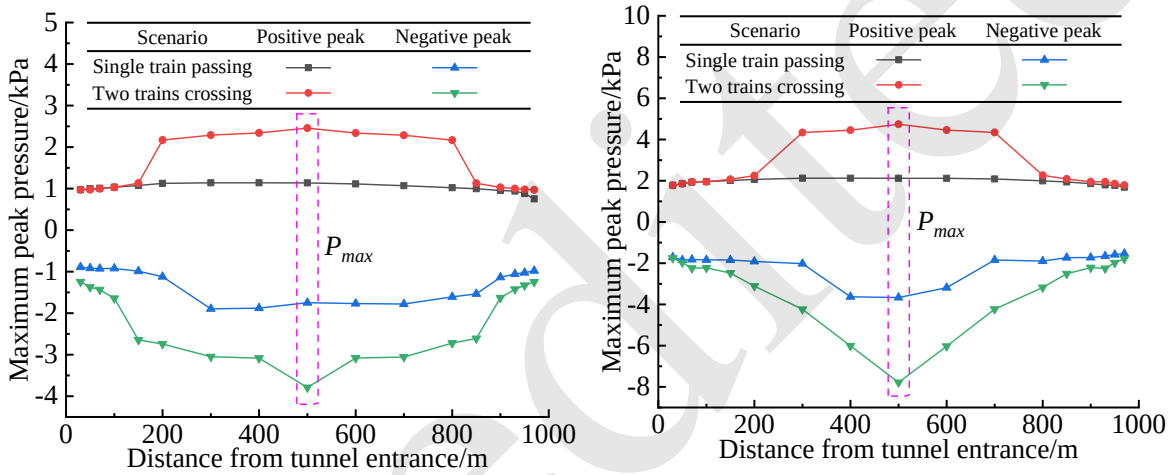

(a) v=275 km/h (b) v=375 km/h

Fig. 11. Distributions of maximum peak pressure along the tunnel longitudinal axis at train speeds of 275 and 375 km/h in Stage I (l=1000 m γ=0.110)

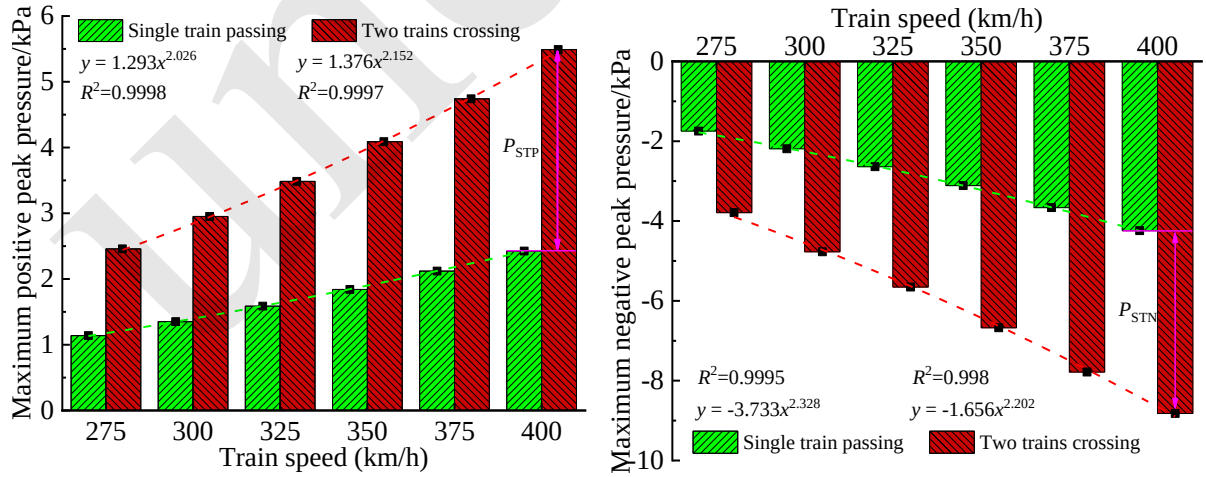

(a) Positive peak pressure (b) Negative peak pressure

Fig. 12. Histogram of maximum peak pressure in the tunnel's longitudinal middle section at different train speeds in Stage I (l=1000 m γ=0.110)

unedited

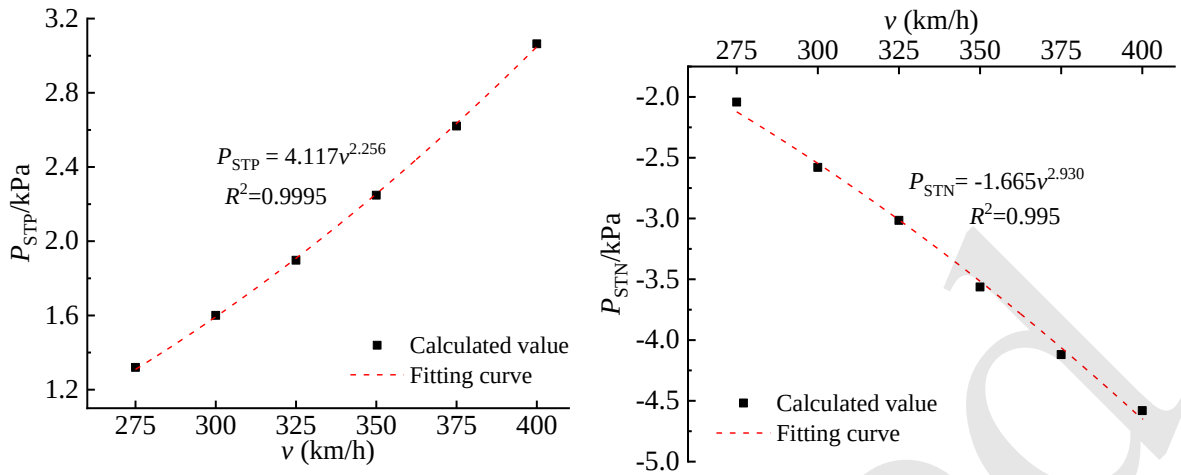

(a) Positive peak pressure **(b) Negative peak pressure**

Fig. 13. Relationship between P_{STP}/P_{STN} and train speed (v) in Stage I (l=1000 m γ=0.110)

(2) Aerodynamic pressure in Stage II

Table 3 shows the MPP/MNP pressures in the tunnel's longitudinal middle section at different train speeds in Stage II (l=1000 m γ=0.110). There is no approximate linear relationship between the amplitude of MPP/MNP pressures or between the P_{STP}/P_{STN} and the power of train speed. The MPP/MNP pressures increase with increasing train speed between 275 and 350 km/h. When train speed increases from 350 to 400 km/h, the MPP/MNP pressures first decrease and then increase.

Table 3 Maximum peak pressures in the tunnel's longitudinal middle section at different train speeds in Stage II (l=1000 m γ=0.110)

Train speed (km/h)		275	300	325	350	375	400
Maximum positive peak pressure (kPa)	Single-train case	1.40	2.06	2.52	2.91	1.71	1.83
	Two-train case	2.85	4.32	4.98	5.74	3.93	4.16
Pressure difference (P_{STP}) (kPa)		1.45	2.26	2.46	2.83	2.22	2.33
Maximum negative peak pressure (kPa)	Single-train case	-1.42	-1.89	-2.32	-2.68	-1.65	-1.55
	Two-train case	-3.04	-4.06	-4.67	-5.29	-3.66	-3.91
Pressure difference (P_{STN}) (kPa)		-1.62	-2.17	-2.35	-2.61	-2.01	-2.36

4.3 Tunnel length effect l

Fig. 14 shows the MPP/MNP pressure distributions along the tunnel's longitudinal axis with tunnel lengths of 400 and 800 m in Stage I (v=350 km/h γ=0.110). The influence of tunnel length on the distributions of the MPP/MNP pressures is similar to that of train speed, i.e. the MPP/MNP pressures and the P_{STP}/P_{STN} arrive at their maximum values at the tunnel's middle section. The histograms of MPP/MNP pressures in the tunnel's longitudinal middle section at different tunnel lengths in Stage I and Stage II are shown in Fig. 15 and Fig. 16, respectively. Compared with the single-train case, the MPP/MNP pressures increase significantly in the two-train case. Table 4 shows the P_{STP}/P_{STN} at different tunnel lengths in Stages I and II. The MPP/MNP pressures of two trains, as well as the P_{STP}/P_{STN}, first increase and then decrease with the increase of tunnel length in Stage I. There is a volatile relationship between the MPP/MNP pressures in the two-train case as well as the P_{STP}/P_{STN} and the tunnel length in Stage II. However, the common phenomenon is that the MPP/MNP pressures in the two-train case and the P_{STP}/P_{STN} arrive at their maximum values when the tunnel length is between 600 and 800 m in Stages I and II.

Based on the analysis above, we can conclude that when two trains are running in double-track tunnel, that the MPP/MNP pressures arrive at their maximum values when the tunnel is between 600 m and 800 m long, which is quite close to the calculation result (710 m) of British Standard EN14067-5 (ref.). The formula of the most unfavorable tunnel length ($l_{tu,crit}$) can be expressed as follows:

unedited

$$l_{tu,crit} = \frac{c}{2}\left(\frac{L_{tr,1}}{v_{tr,1}} + \frac{L_{tr,2}}{v_{tr,2}}\right) \quad (1)$$

where c is the sound speed. $L_{tr,1}$ and $L_{tr,2}$ are the lengths (203 m) of trains 1 and 2. $v_{tr,1}$ and $v_{tr,2}$ are the speeds (350 km/h) of trains 1 and 2.

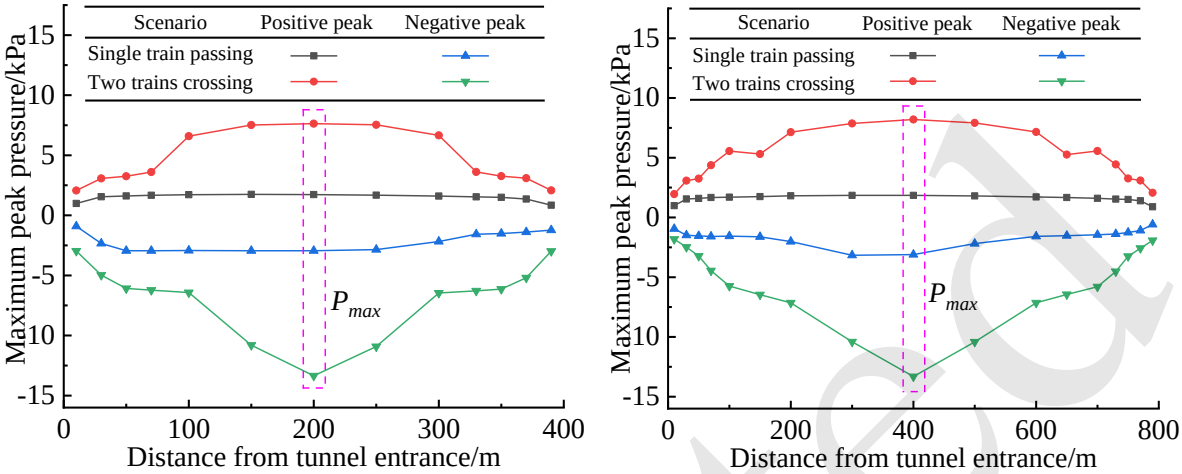

(a) l=400 m **(b) l=800 m**

Fig. 14. Maximum peak pressure along the tunnel's longitudinal axis with tunnel lengths of 400 and 800 m in Stage I (v=350 km/h γ=0.110)

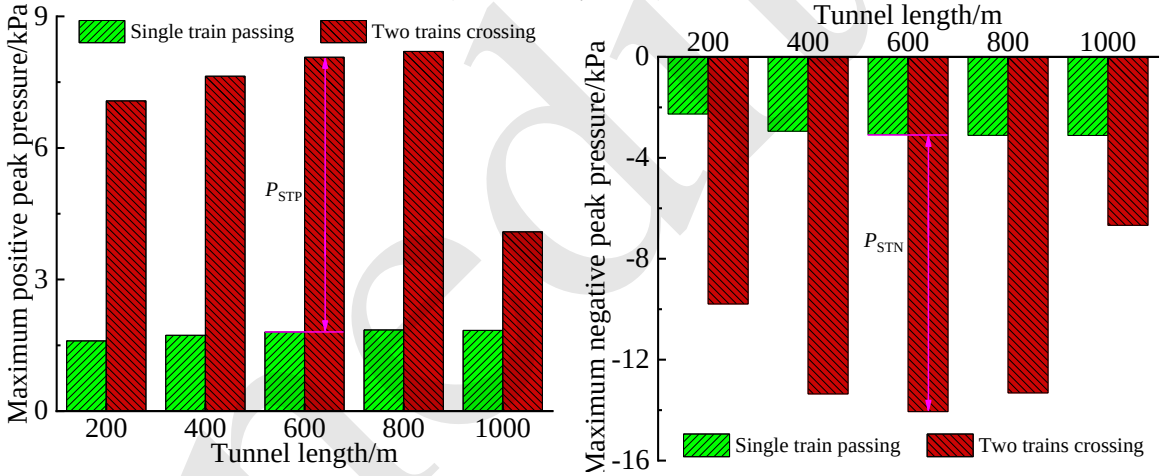

(a) Positive peak pressure **(b) Negative peak pressure**

Fig. 15. Histogram of maximum peak pressure in the tunnel's longitudinal middle section with different tunnel lengths in Stage I (v=350 km/h γ=0.110)

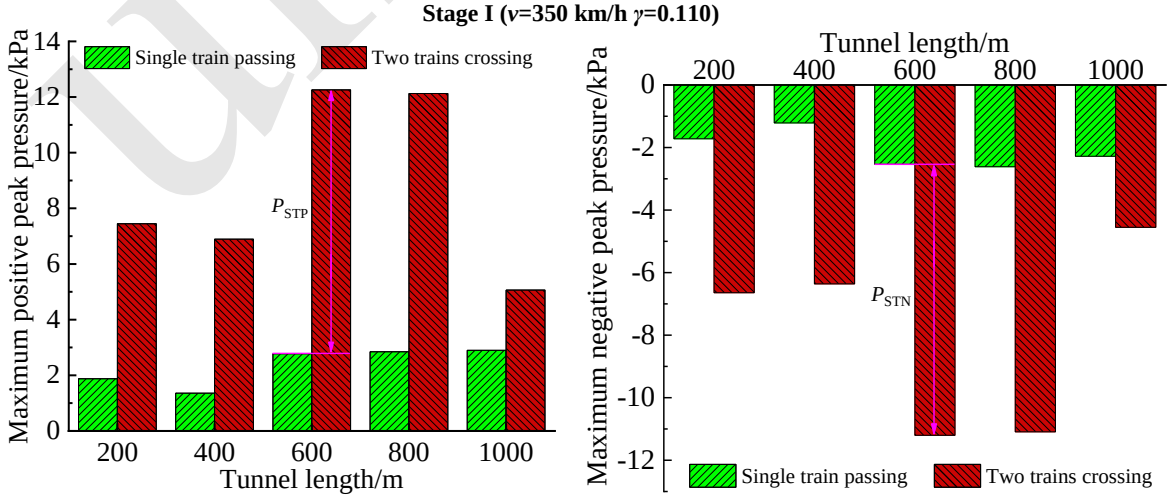

(a) Positive peak pressure **(b) Negative peak pressure**

unedited

Fig. 16. Histogram of maximum peak pressure in the tunnel's longitudinal middle section with different tunnel lengths in Stage II (v=350 km/h γ=0.110)

Table 4 PSTP/PSTN in the longitudinal middle section with different tunnel lengths (v=350 km/h r=0.110)

Tunnel length/m		200	400	600	800	1000
Stage I	P_{STP}/kPa	5.47	5.91	6.26	6.35	2.25
	P_{STN}/kPa	-7.53	-10.41	-10.98	-10.21	-3.56
Stage II	P_{STP}/kPa	5.57	5.54	9.48	9.28	2.17
	P_{STN}/kPa	-4.92	-5.15	-8.67	-8.48	-2.27

4.4 Blockage ratio effect r

Fig. 17 shows the MPP/MNP pressure distributions along the tunnel's longitudinal axis with blockage ratios of 0.0801 and 0.0863 in Stage I (v=350 km/h l=1000 m). The influence of blockage ratio on the distributions of the MPP/MNP pressures is similar to that of train speed and tunnel length. The histogram of MPP/MNP pressures in the tunnel's longitudinal middle section with different blockage ratios in Stages I and II are shown in Figs. 18 and19, respectively. The variation law of aerodynamic pressure with blockage ratio for the single-train case is similar to that for the two-train case. In stage I, the MPP and MNP pressures increase with the increase in the blockage ratio in both cases, and there is an approximately linear relationship between the P_{STP}/P_{STN} and the blockage ratio raised to the power from 2.186 to 2.527. In stage II, the MPP and MNP pressures increase with the increase in the blockage ratio for both cases, and there is an approximately linear relationship between the P_{STP}/P_{STN} and the blockage ratio raised to the power from 2.034 to 2.114. The relationship between the P_{STP}/P_{STN} and the blockage ratio in Stages I and II are respectively shown in Figs. 20 and 21. Whether in Stage I or Stage II, the MPP/MNP pressures and the P_{STP}/P_{STN} increase with the blockage ratio. The amplitude of the MPP/MNP pressures, as well as the P_{STP}/P_{STN}, increase with the blockage ratio raised to the power from 2.032 to 2.798.

The relationships between MPP/MNP, as well as the corresponding pressure difference (P_{STP}/P_{STN}) in the tunnel's longitudinal middle section and influencing factor (v, l, r) in Stage I and Stage II, are shown in Table 5. The subscript i denotes the label of MPP, MNP, STP, and STN. The labels α, β, γ, and δ are the corresponding constants.

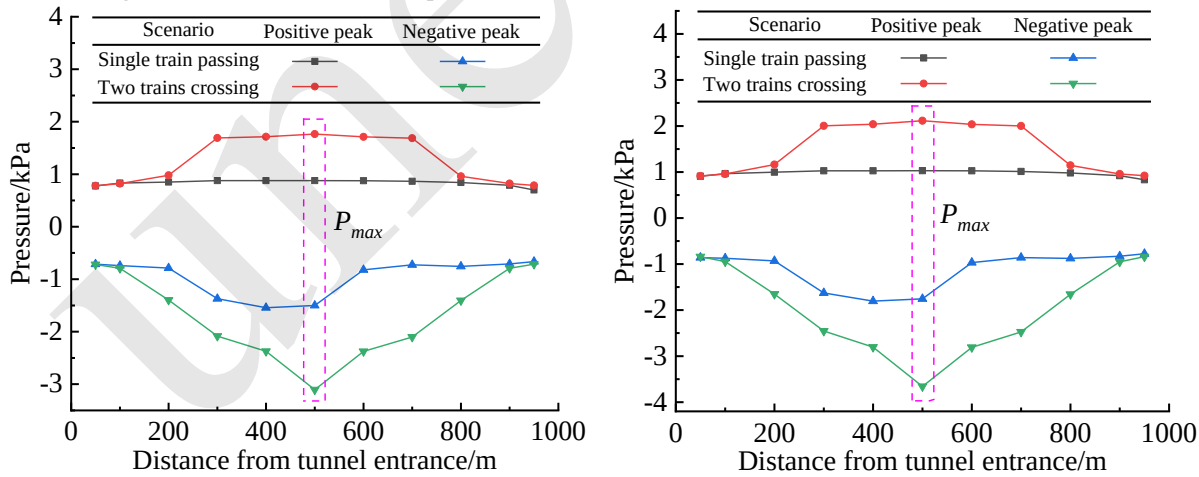

(a) γ=0.0801 **(b) γ=0.0863**

Fig. 17. Maximum peak pressure along the tunnel's longitudinal axis with blockage ratios of 0.0801 and 0.0863 in Stage I (v=350 km/h l=1000 m)

unedited

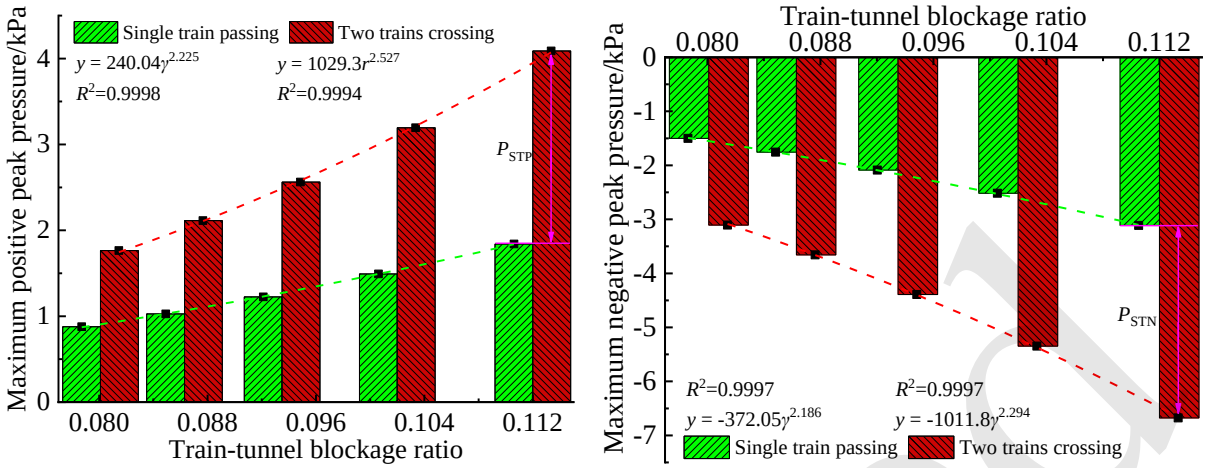

(a) Positive peak pressure **(b) Negative peak pressure**

Fig. 18. Histogram of maximum peak pressure in the tunnel's longitudinal middle section with different blockage ratios in Stage I (*v*=350 km/h *l*=1000 m)

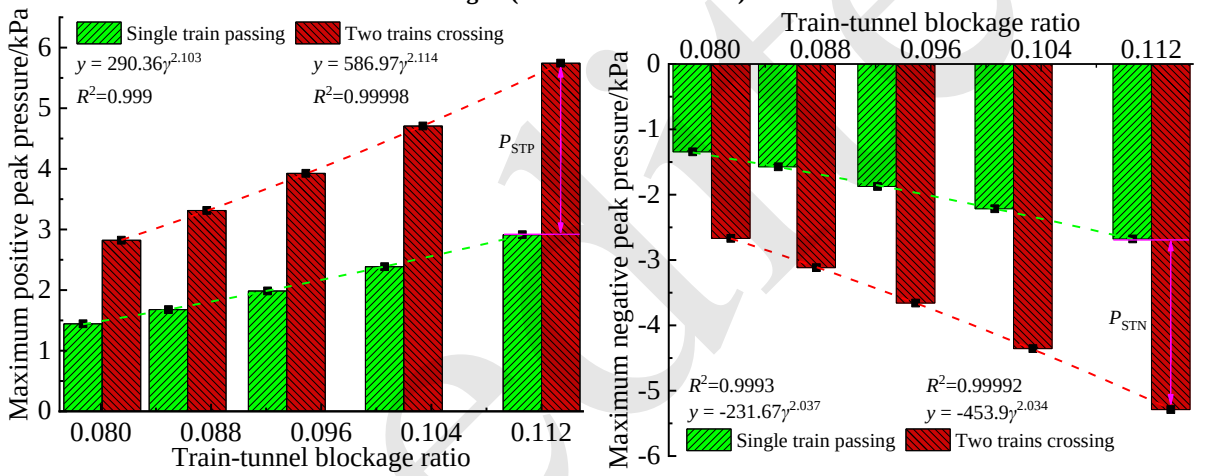

(a) Positive peak pressure **(b) Negative peak pressure**

Fig. 19. Histogram of maximum peak pressure in the tunnel's longitudinal middle section with different blockage ratios in Stage II (*v*=350 km/h *l*=1000 m)

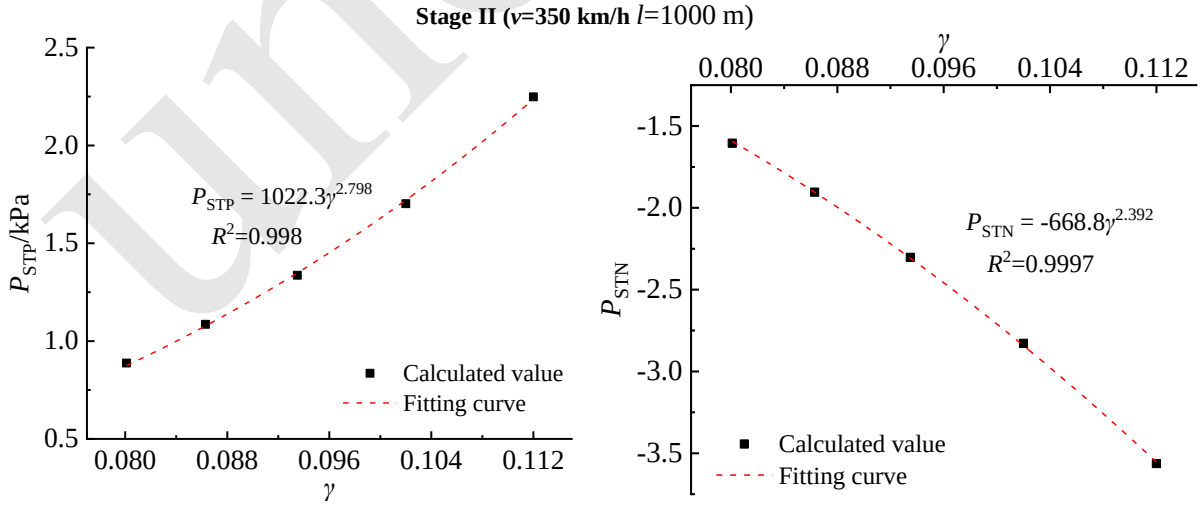

(a) Positive peak pressure **(b) Negative peak pressure**

Fig. 20. Relationship between PSTP/PSTN and blockage ratio (*γ*) in Stage I (*v*=350 km/h *l*=1000 m)

unedited

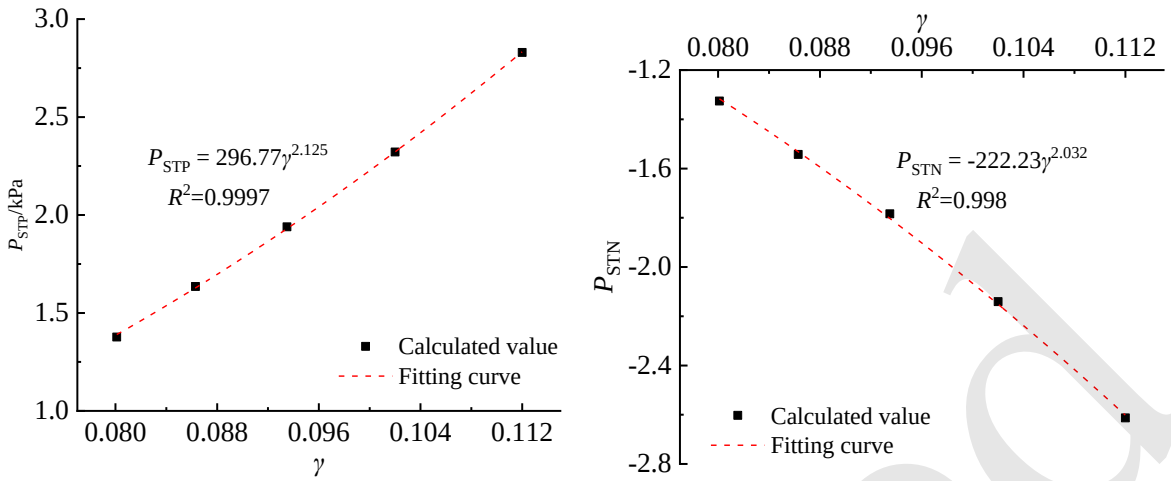

(a) Positive peak pressure **(b) Negative peak pressure**

Fig. 21. Relationship between PSTP/PSTN and blockage ratio (γ) in Stage II (v=350 km/h l=1000 m)

The relationships between MPP/MNP, as well as the corresponding pressure difference (P_{STP}/P_{STN}) in the tunnel's longitudinal middle section and influencing factor (v, l, r) in Stage I and Stage II, are shown in Table 5. The subscript i denotes the label of MPP, MNP, STP, and STN. The labels α, β, γ, and δ are the corresponding constants.

Table 5 Relationship between maximum peak pressure (MPP/MNP) and corresponding pressure difference (P_{STP}/P_{STN}) in the tunnel's longitudinal middle section, and influencing factor (v, l, r)

Influencing factor	Stage I	Stage II
v (275～400 km/h)	$P_i=\alpha v^{\beta}$	P_i increase with increasing v (275～350 km/h), P_i decrease first and then increase with increasing v (350～400 km/h)
l (200～1000 m)		Stronger volatility between P_i and l
r (0.0801～0.1122)		$P_i=\gamma r^{\delta}$

4.5 Engineering application

Affected by the aerodynamic pressure induced by high-speed trains travelling through a tunnel, microcracks in the tunnel lining continue to extend, expand, and interpenetrate, eventually leading to partial shedding. Shedding of the tunnel lining may affect the safe operation of high-speed trains in the tunnel.

Some analytical methods of examining the residual life of tunnel linings under aerodynamic pressure have been proposed (Liu et al., 2019b; Du et al., 2021). In this study, we looked at the influence of various factors of trains and tunnels on aerodynamic pressure. Therefore, the relationship between the residual life of tunnel lining and factors related to trains and tunnels can now be explored. After determining the model, marshalling form, and speed of a train, as well as the length and cross-sectional area of the tunnel, engineers should be able to predict the residual life of the lining of a high-speed railway tunnel.

5 Conclusions

The main conclusions that can be drawn from this study are:

(1) Aerodynamic pressure variation can be divided into Stage I and Stage II, according to the change trend of the time-history curve. Stage I corresponds to irregular pressure fluctuations before the train tail leaves the tunnel exit, and Stage II corresponds to periodic pressure decline after the train tail leaves the tunnel exit. The aerodynamic pressures jump or drop simultaneously for both single-train and two-train cases. The pressure amplitude of the positive and negative peak values in the two-train case is larger than that in the single-train case.

(2) There is an approximately linear relationship between P_{STP}/P_{STN} and train speed raised to the power from 2.256 to 2.930 in Stage I. The P_{STP}/P_{STN} first decreases and then increases with the increase in train speed in Stage II.

(3) The P_{STP}/P_{STN} first increases and then de-

Unedited

creases with the increase in tunnel length in Stage I. There is a volatile relationship between the P_{STP}/P_{STN} and tunnel length in Stage II.

(4) In both Stages I and II, the P_{STP}/P_{STN} increases with the blockage ratio. There is an approximately linear relationship between the P_{STP}/P_{STN} and the blockage ratio raised to the power from 2.032 to 2.798.

Acknowledgments

This work is supported by the Key Project of High-speed Rail Joint Fund of National Natural Science Foundation of China (No. U1934210).

Author contributions

Jianming DU conducted the numerical calculation and wrote the first draft of the manuscript. Qian FANG revised the final version. Xuan ZHANG, and Hualao WANG processed the data.

Conflict of interest

Jianming DU, Qian FANG, San ZHANG, Xuan ZHANG, and Hualao WANG declare that they have no conflict of interest.

References

Cao YL, Chu CR, Chien SY, Wang CY, et al., 2014. Numerical simulation of two trains intersecting in a tunnel. *Tunnelling and Underground Space Technology*, 42: 161-174.
http://dx.doi.org/10.1016/j.tust.2014.02.013

Chen ZW, Liu TH, Zhou XS, et al., 2017(a). Impact of ambient wind on aerodynamic performance when two trains intersect inside a tunnel. *Journal of Wind Engineering and Industrial Aerodynamics*, 169: 139-155.
http://dx.doi.org/10.1016/j.jweia.2017.07.018

Chen XD, Liu TH, Zhou XS, et al., 2017(b). Analysis of the aerodynamic effects of different nose lengths on two trains intersecting in a tunnel at 350 km/h. *Tunnelling and Underground Space Technology*, 66: 77-90.
http://dx.doi.org/10.1016/j.tust.2017.04.004

Deng E, Yang WC, He XH, et al., 2020. Transient aerodynamic performance of high-speed trains when passing through an infrastructure consisting of tunnel–bridge–tunnel under crosswind. *Tunnelling and Underground Space Technology*, 102: 103440.
https://doi.org/10.1016/j.tust.2020.103440

Du J, Zhang L, Yang MZ, et al., 2020. Moving model experiments on transient pressure induced by a high-speed train passing through noise barrier. *Journal of Wind Engineering and Industrial Aerodynamics*, 204: 104267.
https://doi.org/10.1016/j.jweia.2020.104267

Du JM, Fang Q, Wang G, et al., 2021, Fatigue damage and residual life of secondary lining of high-speed railway tunnel under aerodynamic pressure wave. *Tunnelling and Underground Space Technology*, 111: 103851.
https://doi.org/10.1016/j.tust.2021.103851

Du JM, Fang Q, Wang J, et al., 2022(a). Influences of high-speed train speed on tunnel aerodynamic pressures. *Applied Sciences*, 12: 303.
https://doi.org/10.3390/app12010303

Du JM, Fang Q, Wang G, et al., 2022(b). Aerodynamic effects produced by a high-speed train traveling through a tunnel considering different car numbers. *Symmetry*, 14: 479.
https://doi.org/10.3390/sym14030479

Du JM, Fang Q, Wang, G, et al., 2022(c). Analytical solution of a circular lined tunnel with alterable mechanical property under hydrostatic stress and internal pressure. *Journal of Central South University*, 29(8): 2757-2770.
https://doi.org/10.1007/s11771-022-5097-3

Gong C, Zhu ZD, 2018, Numerical study for the aerodynamic effects of high-speed trains on secondary lining. *Henan Science*, 36(5): 721-727.
https://doi.org/1004-3918（2018）05-0721-07

Howe MS, 2007. The genetically optimized tunnel-entrance hood. *Journal of Fluids and Structures*, 23: 1231-1250.
https://doi.org/10.1016/j.jfluidstructs.2007.06.005

Howe MS, Winslow A, Iida M, et al., 2008. Rapid calculation of the compression wave generated by a train entering a tunnel with a vented hood: Short hoods. *Journal of Sound and Vibration*, 311: 254-268.
https://doi.org/10.1016/j.jsv.2007.09.012

Ko YY, Chen CH, Hoe IT, et al., 2012. Field measurements of aerodynamic pressures in tunnels induced by high speed trains. *Journal of Wind Engineering and Industrial Aerodynamics*, 100: 19-29.
https://doi.org/10.1016/j.jweia.2011.10.008

Li RX, Guan YJ, 2012, Investigation of air pressure pulse when two high-speed trains passing by each other in tunnel. *Journal of Mechanical Engineering*, 48(20): 127-134.
https://doi.org/10.3901/JME.2012.20.127

Liu F, Yao S, Zhang J, et al., 2018. Field measurements of aerodynamic pressures in high-speed railway tunnels. *Tunnelling and Underground Space Technology*, 72: 97-106.
https://doi.org/10.1016/j.tust.2017.11.018

Li WH, Liu TH, Huo XH, et al., 2019. Influence of the enlarged portal length on pressure waves in railway tunnels with cross-section expansion. *Journal of Wind Engineering and Industrial Aerodynamics*, 190: 10-22.
https://doi.org/10.1016/j.jweia.2019.03.031

Liu TH, Jiang ZH, Li WH, et al., 2019(a). Differences in aerodynamic effects when trains with different marshalling forms and lengths enter a tunnel. *Journal of Wind Engineering and Industrial Aerodynamics*, 84: 70-81.
https://doi.org/10.1016/j.tust.2018.10.016

Liu TH, Jiang ZH, Chen XD, et al., 2019(b). Wave effects in a realistic tunnel induced by the passage of high-speed trains. *Tunnelling and Underground Space Technology*, 86: 224-235.

https://doi.org/10.1016/j.tust.2019.01.023
Li WH, Liu TH, Chen ZW et al., 2020. Comparative study on the unsteady slipstream induced by a single train and two trains passing each other in a tunnel. *Journal of Wind Engineering and Industrial Aerodynamics*, 198: 104095. https://doi.org/10.1016/j.jweia.2020.104095
Liu TH, Geng SG, Chen XD, et al., 2020. Numerical analysis on the dynamic airtightness of a railway vehicle passing through tunnels. *Tunnelling and Underground Space Technology*, 97: 103286. https://doi.org/10.1016/j.tust.2020.103286
Li XH, Deng J, Chen DW, et al., 2021. Unsteady simulation for a high-speed train entering a tunnel. *Journal of Zhejiang University-Science A (Applied Physics & Engineering)*, 12(12): 957-963. https://doi.org/10.1631/jzus.A11GT008
Lu YB, Wang TT, Yang MZ, et al., 2021. The influence of reduced cross-section on pressure transients from high-speed trains intersecting in a tunnel. *Journal of Wind Engineering and Industrial Aerodynamics*, 201: 104161. https://doi.org/10.1016/j.jweia.2020.104161
Rivero JM, Gonzalez-Martínez E, Rodríguez-Fernandez M., 2018. Description of the flow equations around a high speed train inside a tunnel. *Journal of Wind Engineering and Industrial Aerodynamics*, 172: 212-229. https://doi.org/10.1016/j.jweia.2017.09.012
Saito S, 2019. Optimizing cross-sectional area of tunnel entrance hood for high speed rail. *Journal of Wind Engineering and Industrial Aerodynamics*, 184: 296-304. https://doi.org/10.1016/j.jweia.2018.11.028
Saito S, Fukuda T, 2020. Design of a tunnel entrance hood for high-speed trains. *Journal of Wind Engineering and Industrial Aerodynamics*, 206: 104375. https://doi.org/10.1016/j.jweia.2020.104375
Niu JQ, Zhou D, Liu TH, et al., 2017. Numerical simulation of aerodynamic performance of a couple multiple units high-speed train. *International Journal of Vehicle Mechanics and Mobility*, 55(5): 681-703. http://dx.doi.org/10.1080/00423114.2016.1277769
National Railway Administration of the People's Republic of China. 2018. Railway applications—Aerodynamics—Part 4: Requirements for train aerodynamic simulation. TB/T3503.4. Beijing: China Railway Publishing House Co., Ltd.
Wang TT, Wu F, Yang MZ, et al., 2018. Reduction of pressure transients of high-speed train passing through a tunnel by cross-section increase. *Journal of Wind Engineering and Industrial Aerodynamics*, 183: 235-242. https://doi.org/10.1016/j.jweia.2018.11.001
Yang QS, Song JH, Yang WC, 2016. A moving model rig with a scale ratio of 1/8 for high speed train aerodynamics. *Journal of Wind Engineering and Industrial Aerodynamics*, 152: 50-58. http://dx.doi.org/10.1016/j.jweia.2016.03.002
Zhang L, Yang MZ, Liang XF, et al., 2017. Oblique tunnel portal effects on train and tunnel aerodynamics based on moving model tests. *Journal of Wind Engineering and Industrial Aerodynamics*, 167: 128-139. http://dx.doi.org/10.1016/j.jweia.2017.04.018

中文概要

题　目：高速铁路隧道内单车经过与双车交会诱发的气动特性对比分析

作　者：杜建明[1]，房倩[2]，张翾[1]，王华牢[1]
机　构：[1]交通运输部公路科学研究所 桥梁隧道研究中心，北京 100088；[2]北京交通大学 隧道及地下工程教育部工程研究中心，北京 100044

目　的：气动压力是高速铁路隧道结构服役性能的重要影响因素之一。文章旨在对比高速铁路隧道内单车经过与双车交会诱发的气动压力差异特征，探究列车速度、隧道长度以及阻塞比对气动压力差异特征的影响规律，进而为高铁隧道结构后续的科学服役提供理论支撑。

创新点：1. 对比分析了高速铁路隧道内单车经过与双车交会诱发的气动压力差异特征；2. 探究了列车速度、隧道长度以及阻塞比对气动压力差异特征的影响规律。

方　法：1. 采用三维数值仿真，再现了高速列车经过隧道的全过程。通过与现场实测数据进行对比，验证了三维数值仿真所用模型参数的准确性与合理性；2. 通过数理统计，对比了高铁隧道内单车经过与双车交会诱发的气动压力差异特征，探究了列车速度、隧道长度以及阻塞比对气动压力差异特征的影响规律。

结　论：1. 高速铁路隧道内单车经过与双车等速交会时，气动压力时程曲线同步升降低，且双车交会诱发的压力峰值显著大于单车经过；2. 列车在隧道内行驶时，气动压力与速度幂次方成正相关性；3. 气动压力峰值与隧道长度幂次方之间无显著的线性关系；4. 列车在隧道内行驶或驶出隧道后，气动压力峰值与阻塞比幂次方均成正相关。

关键词：铁路隧道；气动效应；压力特征；列车速度；隧道长度；阻塞比

unedited